Revealing the arc dynamics in a gliding arc plasmatron: a better insight to improve CO_2 conversion

Reference:

Ramakers Marleen, Medrano Jose A., Trenchev Georgi, Gallucci Fausto, Bogaerts Annemie.- Revealing the arc dynamics in a gliding arc plasmatron: a better insight to improve CO_2 conversion

Plasma sources science and technology / Institute of Physics [Londen] - ISSN 0963-0252 - 26:12(2017), 125002

Full text (Publisher's DOI): https://doi.org/10.1088/1361-6595/AA9531

To cite this reference: https://hdl.handle.net/10067/1470230151162165141

Revealing the arc dynamics in a Gliding Arc Plasmatron: A better insight to improve CO_2 conversion

Marleen Ramakers[a,*], Jose A. Medrano[b], Georgi Trenchev[a], Fausto Gallucci[b] and Annemie Bogaerts[a]

[a] Research group PLASMANT, Department of Chemistry, University of Antwerp, Universiteitsplein 1, BE-2610 Antwerp, Belgium
[b] Chemical Process Intensification, Department of Chemical Engineering and Chemistry, Eindhoven University of Technology, De Rondom 70, 5612AP Eindhoven, The Netherlands

Abstract

A Gliding Arc Plasmatron (GAP) is very promising for CO_2 conversion into value-added chemicals, but to further improve this important application, a better understanding of the arc behavior is indispensable. Therefore, we study here for the first time the dynamic arc behavior of the GAP by means of a high-speed camera, for different reactor configurations and in a wide range of operating conditions. This allows us to provide a complete image of the behavior of the gliding arc. More specifically, the arc body shape, diameter, movement and rotation speed are analyzed and discussed. Clearly, the arc movement and shape relies on a number of factors, such as gas turbulence, outlet diameter, electrode surface, gas contraction and buoyance force. Furthermore, we also compare the experimentally measured arc movement to a state-of-the-art 3D-plasma model, which predicts the plasma movement and rotation speed with very good accuracy, to gain further insight in the underlying mechanisms. Finally, we correlate the arc dynamics with the CO_2 conversion and energy efficiency, at exactly the same conditions, to explain the effect of these parameters on the CO_2 conversion process. This work is important for understanding and optimizing the GAP for CO_2 conversion.
Keywords: Arc dynamics modeling, CO_2 conversion, Gliding Arc Plasmatron, High-speed camera

1. Introduction

Plasmas are being used for several industrial applications, like etching, deposition and surface treatment in materials technology and microelectronics, as lights, lasers, plasma televisions and for medical applications [1]. Besides, they are also extensively applied for environmental applications. In this domain, most research has been carried out on air purification [2,3]. However, in recent years, more and more research is being performed on the conversion of CO_2 into value-added chemicals and fuels [4–26]. Gliding arc plasmas prove to be very promising for the latter application [15,16,27–34].

A classical gliding arc configuration typically consists of two plane diverging electrodes between which a gas flows. By applying a high voltage over the electrodes, an arc discharge arises at the narrowest point. The arc discharge is pushed by the gas flow towards the place where the electrodes diverge. It elongates with rising interelectrode-distance until it extinguishes. In the meantime a new arc appears at the narrowest point and in this way a new cycle starts [28,35,36].

This classical gliding arc configuration, however, has some downsides for applications of gas conversion. Indeed, it is incompatible with various industrial systems because of its 2D geometry, the gas treatment is non-uniform because only a limited fraction of the gas passes through the arc, and

the residence time of the gas inside the plasma is rather short. Therefore, a three-dimensional gliding arc reactor with vortex flow, also called Gliding Arc Plasmatron (GAP), has recently been developed [16]. This reactor can be easily implemented in industry and the specific gas flow configuration forces the gas to pass through the plasma, which also results in a longer residence time.

Although the GAP is very promising for gas conversion, only limited research has been performed to-date [16,23,37–39]. To our knowledge, no studies have been carried out yet on the gliding arc hydrodynamics in a GAP using high-speed imaging. This information, however, is crucial to correlate this behavior with applications of the GAP, such as CO_2 conversion. Furthermore, such information is also very useful for the validation of models of the GAP [37], again to better understand and further improve the applications. Therefore, in this paper we present a study of the arc behavior in a GAP, making use of a high-speed camera, for different reactor configurations, gas flow rates and electrical currents. This provides a complete picture of the behavior of the gliding arc, more specifically, the exact shape and movement of the arc. We will also compare the measured arc movement with computer simulations, to obtain more insight in the underlying mechanisms. Finally, by comparing the results with data obtained for the CO_2 conversion in the GAP in the same range of conditions, we can also provide a better understanding on how this behavior can influence the CO_2 conversion.

2. Methods

2.1 Description of the experiments

The arc dynamics in the Gliding Arc Plasmatron (GAP) are investigated by means of a CMOS high-speed camera. The main objective of this study is to reveal the movement of the arc as a function of different operating conditions, like the anode diameter, the feed flow rate and input current, as reported in Table 1. A photo and a schematic drawing of the GAP are illustrated in figure 1. For these experiments, we used four different stainless steel electrodes, i.e., a high voltage electrode and three grounded electrodes. The high voltage electrode, which acts as the cathode, has a length of 20.30 mm and a diameter of 17.50 mm. All grounded electrodes, acting as anode, have the same length (16.30 mm) but their diameter is 7.08, 14.20 and 17.50 mm, respectively. There is a 3 mm gap between the cathode and anode. A more detailed description can be found in [33]. For all the experiments CO_2 is used as feed gas. Therefore, the results allow an assessment of the influence of the arc dynamics on CO_2 conversion.

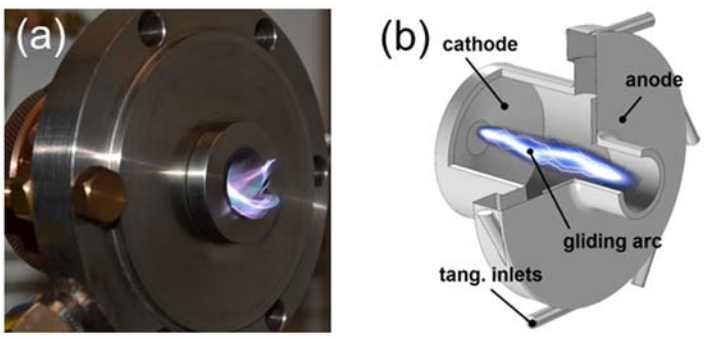

Figure 1. Photograph of the Gliding Arc Plasmatron (GAP) (a) and schematic drawing of the internal structure (b).

The high-speed camera (Phantom SpeedSense 341 model) from DantecDynamics gives a maximum resolution of 2560 by 1600 pixels at a frame rate of 800 Hz, with the possibility to go up to 500 kHz at lower resolutions. For each experiment, the camera settings are first

optimized in order to enhance the detection of the rotating arc. More specifically, the frame rate is selected to properly identify the arc rotation, and the exposure time of the detector is optimized to increase the contrast between the arc and the reactor. Since the arc rotation speed depends mostly on the anode diameter and the feed flow rate, it is important to optimize the recording frequency, so that the arc can be tracked while rotating inside the anode disk. In general, a frame rate of 3.4 kHz is selected for an image resolution of 800 x 800 pixels. Only for those cases where higher frequencies are demanded, like for high rotation speeds, the image resolution is decreased to 288 x 288 pixels, thus leading to recordings with a frame rate of 14 kHz. Similarly, the exposure time of the detector is optimized in order to find the best compromise between the following two properties: on one hand, it should be high enough to achieve sufficient contrast between the plasma and the reactor, so that it is possible to identify and track the plasma movement. On the other hand, since the plasma velocity is rather high, the exposure time should be low enough to avoid the plasma to become blurred due to the plasma movement during the image acquisition. For most of the cases, an exposure time of 5–10 µs is selected. Only in the case of reduced input current (0.05 A) an exposure time of 25 µs is selected.

Table 1. Experimental conditions selected for the plasma dynamics investigation.

Anode diameter (mm)	Feed flow rate (L/min)	Input current (A)	Different views recorded
7.08	10, 16, 22	0.35	Frontal 90° angle
14.20	10, 16, 22	0.35	Frontal 90° angle 45° angle
14.20	10, 16, 22	0.05	Frontal 90° angle
17.50	10, 16, 22	0.35	Frontal 90° angle

To better understand the plasma dynamics inside the reactor, different views of the anode disk are recorded (see figure 2). In particular, the arc rotation speed is calculated from a frontal view of the anode, based on the number of turns measured through the recordings as a function of the recording time. Since the plasma arc can rotate either inside the anode disk or in the outer part of the anode, two other views are recorded as well for selected cases. A 45° view is recorded for the particular case of an anode diameter of 14.20 mm and a feed flow rate of 16 L/min, to provide more information on the plasma behavior and also to obtain a better description for the comparison to the plasma dynamics modeling. The third view corresponds to the lateral recordings of the anode disk. In this case, the camera is aligned perpendicular to the feed gas, leading to a 90° view of the anode. Through these experiments it is possible to visualize the end of the arc in the anode side and to discuss differences observed between the experiments.

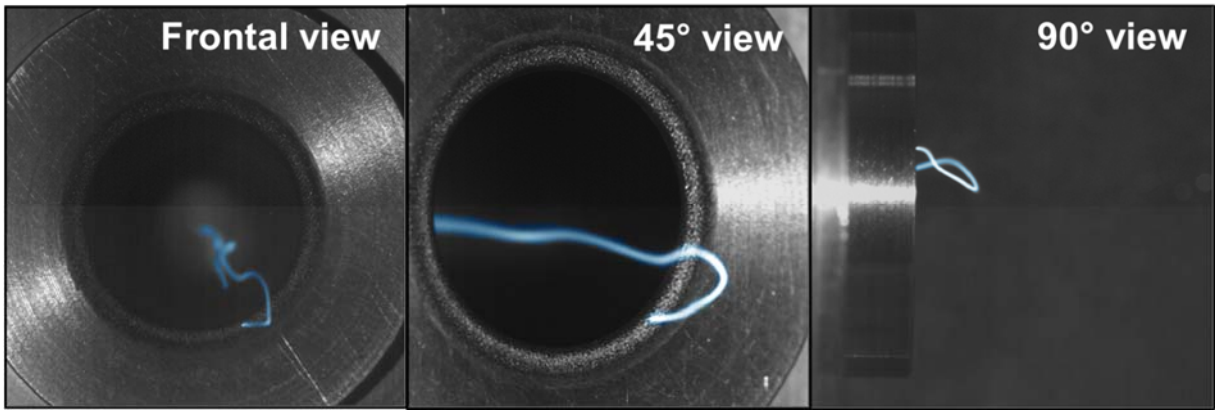

Figure 2. Snapshots of the different views for an anode diameter of 14.20 mm and a feed flow rate of 16 L/min.

The sequence followed for the recordings and post-processing of the data is similar for all the experiments and can be described as follows. At first, the camera is aligned and the lens is focused to the anode disk. Subsequently, the exposure time is selected accordingly to fulfil the two characteristics for a good recording, as mentioned above. Since the exposure time in that case is rather low, the reactor can hardly be identified. Therefore, a second recording is performed with a much higher exposure time (and absence of the arc) to overlap the arc movement with the reactor as background. To do so, the camera is kept aligned to the reactor and the recording is done with external (and homogeneous) illumination provided by two LED lights. The recorded images are analyzed using the commercial software Davis 8.0 from LaVision. The arc diameter and the distance of the plasma to the anode disk in the 90° view are measured by converting first the image pixels into metric units.

In order to gain more insights in the plasma dynamics, statistical analysis of the experimental recordings has been carried out. In particular, a sufficiently long recording sequence (0.5 – 1 s) is applied for all the experiments listed in Table 1, which ensures a realistic representation of time-average results. Statistical analysis is carried out on the rotation speed by splitting the long-recording sequence into shorter ones. To do so, each recording is divided into 10-20 shorter recordings, which allows to elucidate better the arc rotation dynamics, especially in those cases where the arc moves from the inner to the outer part of the anode disk as discussed in the results section.

The average diameter of the arc is measured in the in-focus region, thus next to the anode, for random images at different positions within the anode disk. If the measurement is to be done in the out of focus region, the method would lead to less accurate results since the arc is not well defined. The analysis itself consists in the measurement of the number of pixels in the perpendicular of the arc direction. These pixels are subsequently converted into metric units by a calibration of the image size. The arc behavior in a GAP is a very dynamic process, thus it is important to repeat these measurements over time and at different positions in the anode side to get representative results of the arc properties. Statistics have been obtained by measuring the arc diameter of a minimum of 50 individual images in every experimental condition. Similarly, the average and standard deviation of the arc elongation from the inner to the outer part of the anode is obtained by measuring the longest perpendicular distance of the arc to the anode surface for more than 50 individual images of each recording.

2.2 Description of the modeling work

Complementary to the experiments, a 3D plasma model is developed for the purpose of studying the dynamic characteristics of the GAP. The model geometry is directly taken from the experimental setup. Only the internal structure of the reactor is simulated (see figure 1(b)). The model is developed in 3D for argon, because a 3D model in CO_2 would yield an excessively long computation time. However, from our 2D modeling in both argon and CO_2 [40], we observed no difference in the arc shape, although the plasma characteristics were different (i.e., lower plasma density and higher gas temperature in CO_2). Thus, we may assume that the arc behavior in the argon and CO_2 GAP is quite similar.

The gas flow simulation is performed using the computational fluid dynamics (CFD) module of the Comsol software package [41]. A RANS (Reynolds-Averaged-Navier-Stokes) turbulent model is used, as the rather high flow velocity promotes significant turbulence. More specifically, the model used for the gas flow is the Shear Stress Tensor (SST) model [42]. The details of the model are described in the Supplementary Information.

3. Results and discussion

3.1 Arc behavior at different conditions

As mentioned in Table 1 above, we investigated the arc behavior for three different anode diameters, which give rise to different gas flow vortex patterns. Figure 3 shows snapshots of the arc in the different configurations (i.e., with different anode diameters). The results for the configuration with anode diameter of 14.20 mm are presented at both low (0.05 A) and high (0.35 A) electric current. In general, the arc can be seen as a thin wire with a spiral-like form. However, the arc behaves differently for the three different anode diameters. More specifically, we see a difference in arc diameter, elongation of the arc and rotation speed, as will be elaborated in more detail below.

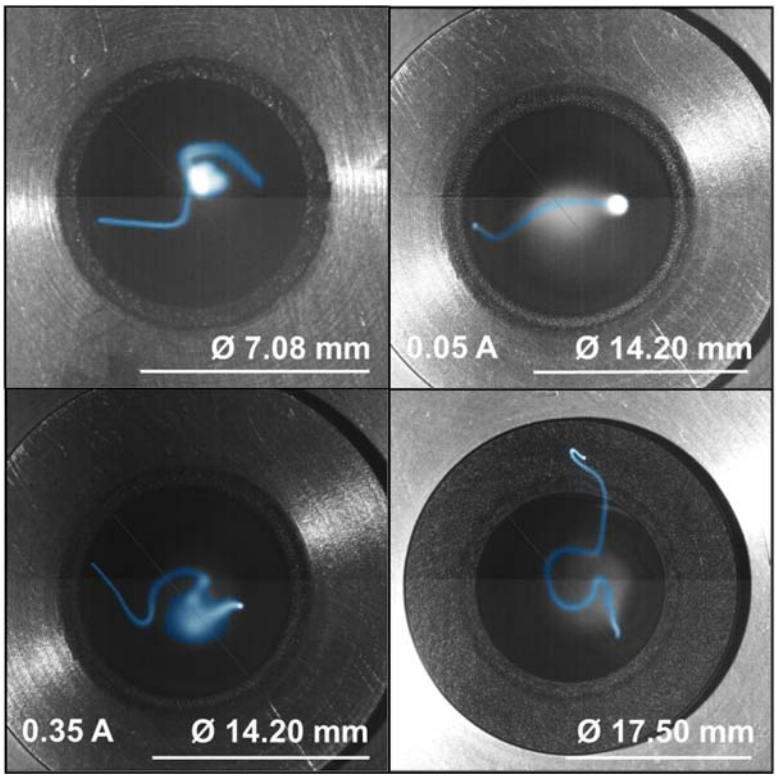

Figure 3. Snapshots of the arc discharge for the three different anode diameters investigated in this work. The top right and bottom left pictures correspond to an input current of 0.05 A and 0.35 A, respectively. The results for the two other anode diameters are at 0.35 A. The gas flow rate is 16 L/min in all cases.

In figure 4, the arc diameter is plotted for the three different anode diameters, and in the case of 14.20 mm diameter also for two different electric currents. It is clear that when the anode diameter increases, the arc diameter rises as well. The arc diameter appears to be rather independent of the electric current in case of the anode diameter of 14.20 mm, but it was visible in the experiment that the arc is less bright for 0.05 A than for 0.35 A. This can be seen in figure 3 as the soft white glow in the center for the 0.05 A case, while for 0.35 A, the glow around the arc is much brighter. The lower electric current will lead to less excitation and thus less bright plasma. We can conclude that these two cases correspond to different regimes of the arc, as was also demonstrated in [33]. Furthermore, our experiments also revealed that changing the gas flow rate will not change the arc diameter.

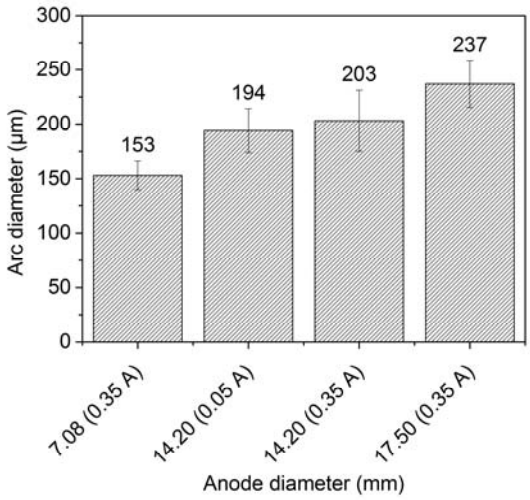

Figure 4. Arc diameter for the three different anode diameters, and in the case of 14.20 mm also for two different electric currents. The arc diameter does not depend on the feed flow rate for each anode diameter.

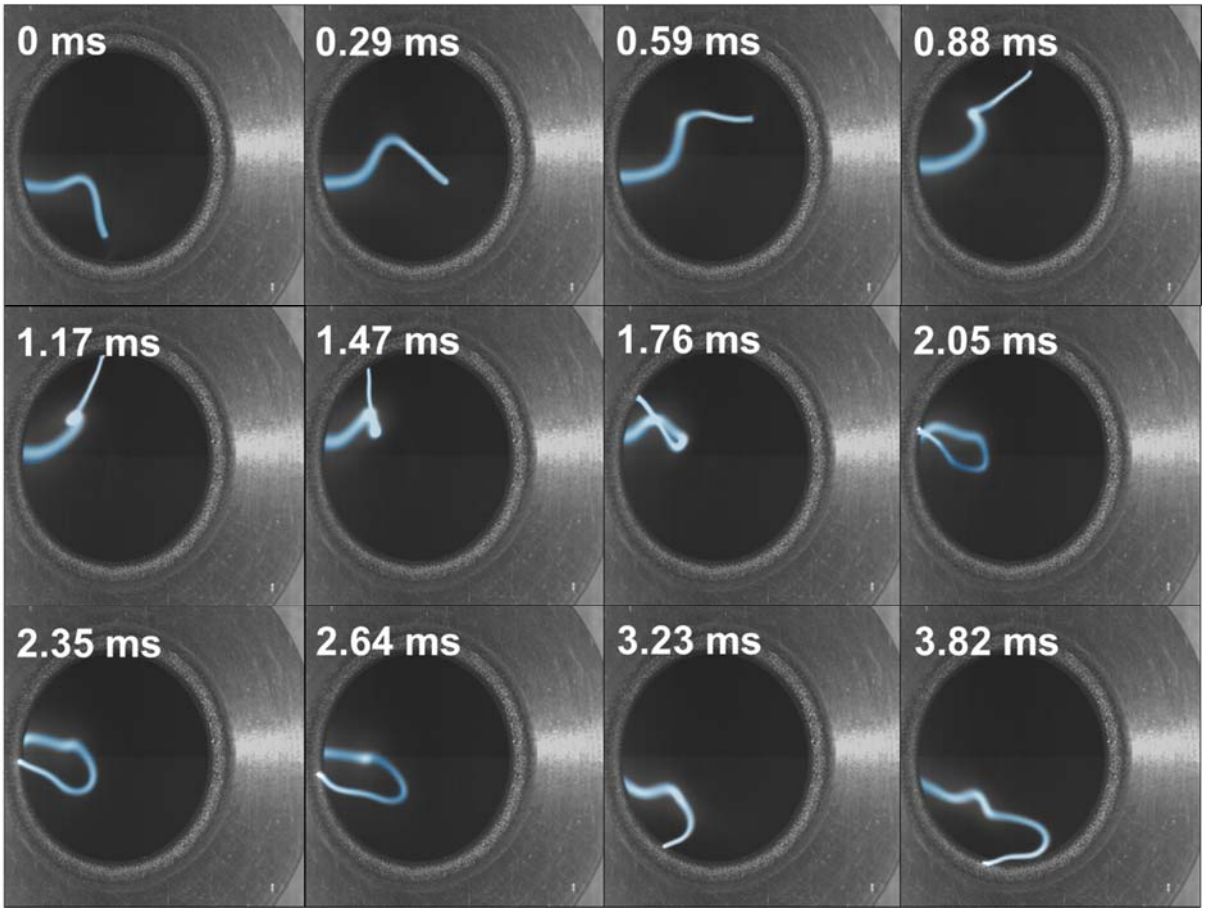

Figure 5. Snapshots at different times in the arc rotation for an anode diameter of 14.20 mm and an inlet gas flow rate of 16 L/min from a side view of 45°. It is observed how the arc moves from the inner part of the anode to the external face of the anode disk.

Figure 5 shows snapshots at different times in the arc rotation for an anode diameter of 14.20 mm and a gas flow rate of 16 L/min from a side view of 45°. It can be observed that the arc moves from the inner part of the anode to the external face of the anode disk. This is also the case for the other

configurations. However, we observe another phenomenon in the case of the configurations with anode diameter of 14.20 mm and 17.50 mm, that is not present in the configuration with anode diameter of 7.08 mm. In the first two cases, the anchor point of the arc at the anode moves along the external face of the anode disk towards the outer diameter of the anode, which has the same dimension for all the configurations. When the inner anode diameter increases, the arc moves further away from the inner diameter, as can be seen in movies 1 and 2, for the configurations with anode diameter of 14.20 mm and 17.50 mm, respectively (see Supplementary Information). In these cases the arc not only elongates from the inner part of the anode to the external face of the anode disk (as illustrated in figure 5) but also along the external face of the anode disk towards the outer diameter of the anode. This can have consequences for the gas mixing and therefore also for the CO_2 conversion, which will be explained below.

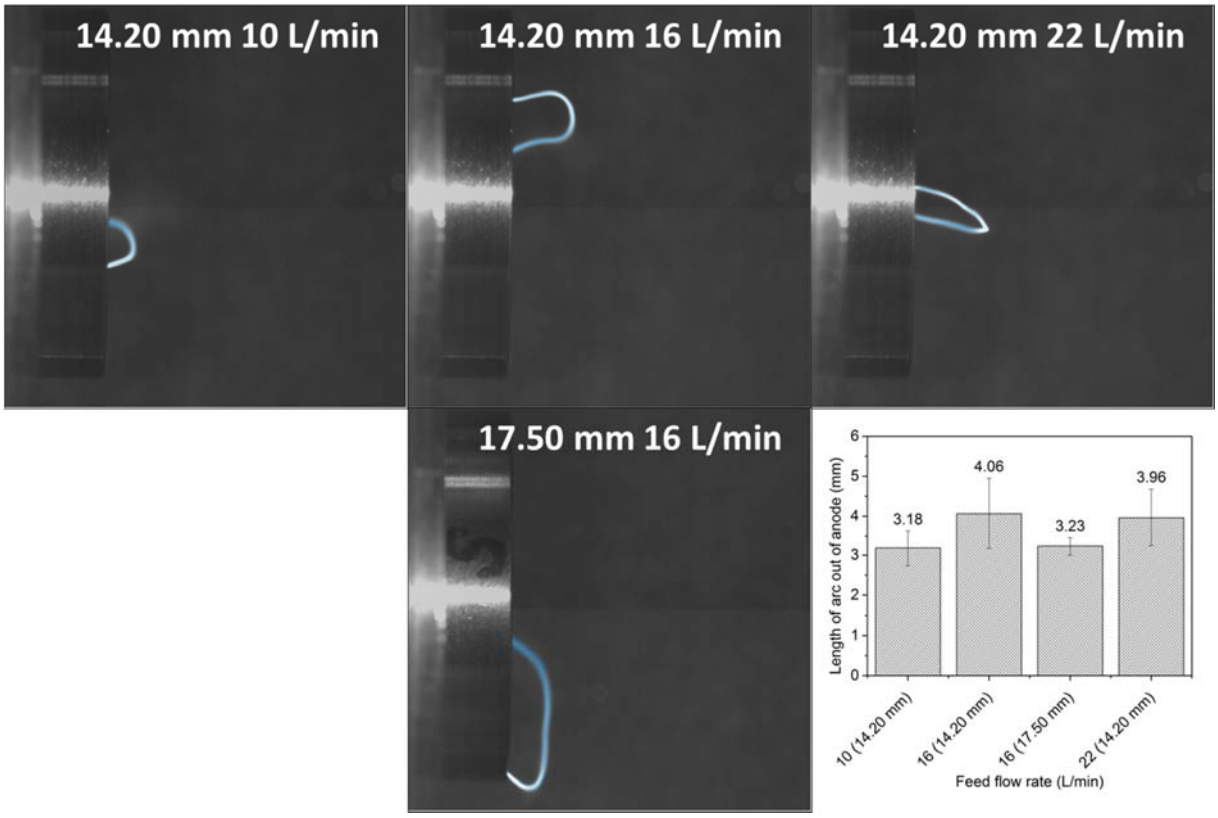

Figure 6. Snapshots of the arc discharge for an anode diameter of 14.20 mm (and gas flow rate of 10, 16, 22 L/min) and 17.50 mm (16 L/min) from a side view of 90°, as well as a graph with the length of the arc out of the anode, plotted as a function of the gas flow rate.

Because of the movement of the anchor point of the arc along the external face of the anode disk, the arc comes out of the reactor, which can be seen in figure 6. This is only the case for the configurations with anode diameters of 14.20 mm and 17.50 mm. In the configuration with anode diameter of 7.08 mm, the arc does not leave the reactor. In figure 6, the length of the arc that comes out of the anode is also plotted as a function of the gas flow rate. When the gas flow rate is increased from 10 to 16 L/min in the configuration with anode diameter of 14.20 mm, the length of the arc coming out of the reactor also increases. However, if we increase the gas flow rate even further to 22 L/min, the arc length does not change anymore. If we compare the configurations with anode diameter of 14.20 mm and 17.50 mm, we see that for a gas flow rate of 16 L/min, the length of the arc is smaller for a larger anode diameter. Moreover, if we compare the case with an anode diameter

of 14.20 mm at a gas flow rate of 10 L/min with the case with an anode diameter of 17.50 mm at a gas flow rate of 16 L/min, the length of the arc is similar. These observations can both be explained by the fact that for the configuration with anode diameter of 17.50 mm, the arc elongates more towards the outer diameter of the anode instead of lengthwise.

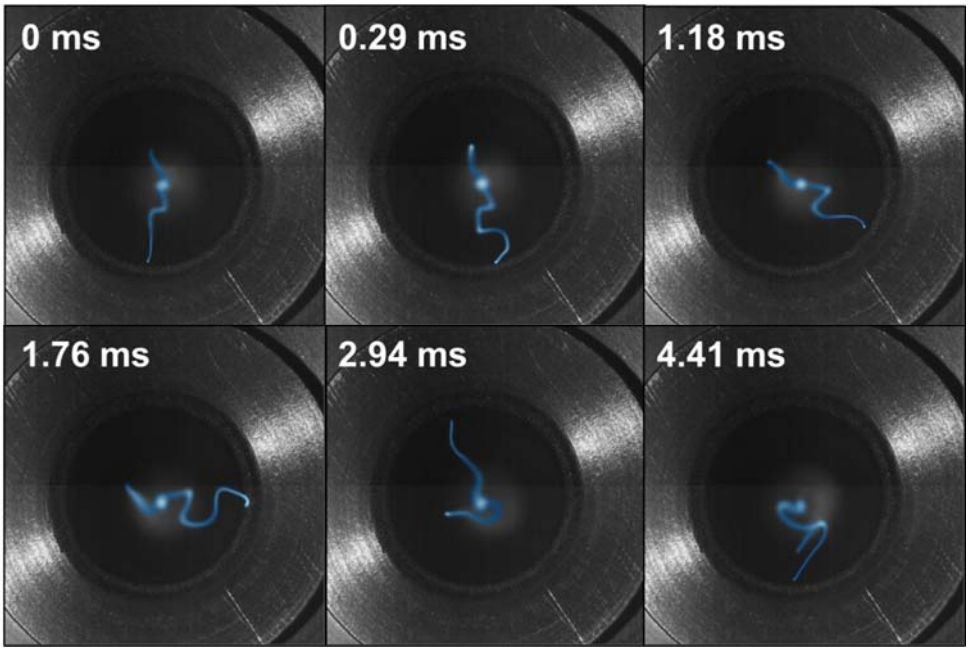

Figure 7. Snapshots at different times in the arc rotation for an anode diameter of 14.20 mm and an inlet gas flow rate of 16 L/min.

Besides the difference in arc diameter and elongation of the arc, also the rotation speed depends on the anode diameter. Snapshots at different times in the arc rotation for an anode diameter of 14.20 mm at a gas flow rate of 16 L/min are shown in figure 7. The rotation is also visualized in movie 3 in the Supplementary Information, where it is clearly observed that the arc "hops" around the electrodes. It seems that the arc movement is dominated by reattachment on the electrodes and it does not follow a stable rotation. Therefore, the calculated rotation speed is only indicative. In figure 8 the rotation speed is plotted as a function of the gas flow rate, for the three different anode diameters, as well as two different currents in case of the 14.20 mm anode diameter. The rotation speed significantly increases upon smaller anode diameter. Furthermore, in the case of 7.08 mm anode diameter, the rotation speed clearly increases with increasing gas flow rate, while this trend is less pronounced in the configurations with anode diameter of 14.20 mm and 17.50 mm. In case of 14.20 mm anode diameter at an input current of 0.05 A, we even see a decrease of rotation speed with increasing gas flow rate. The reason is that at 10 L/min, the arc rotates more smoothly as compared to the other gas flow rates, where we observed that the arc jumps backwards with a corresponding decrease in the rotation speed.

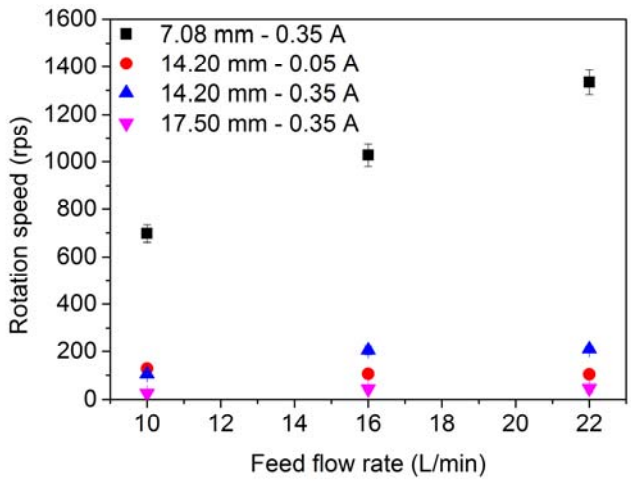

Figure 8. Rotation speed plotted as a function of gas flow rate, for the three different anode diameters, as well as two different currents for the anode diameter of 14.20 mm.

The dependence of the arc behavior on the different parameters can be explained based on the gas flow dynamics. First, gas flow rates and flow speed are directly linked to flow turbulence. Turbulence stands for small, local oscillations in flow speed, pressure and density, accompanied with turbulent "vortices" [43]. These vortices are an essential part of the gas flow and will directly affect the arc shape by bending it into complex forms. Clearly, this has an impact on the arc length, which is linked with the overall dynamics of the arc, as the plasma conducts the electricity in the circuit, i.e. voltage, current and power will depend on the fluid dynamics. Using different anode diameters has a clear impact on the gas flow speed, and therefore, on the arc movement, and this is evident in the experiments. Furthermore, the mechanics of the arc also depend on factors such as electrode surface and temperature. Small bumps and scratches on the electrode caused by machining and natural wear can cause a local increase of the electric field, and attract the arc. Random arc jumps are indeed visible in the experiments, and they are attributed to this very factor. Moreover, as the arc remains at one spot for a longer time period, it will "drill" even more holes on the electrode surface, eventually making a "hot spot". Normally, the arc will remain attached there in an "anchored" state, causing damage to the cathode. When this was observed in our experiments, the cathode was replaced. Therefore, we believe that the effect of cathode wear was minor in our experiments, compared to the effect of the arc current, gas flow rate and anode diameter. The arc current can also cause numerous changes in the arc its behavior. First, higher current will contribute to higher Joule heating of the arc, and affect its temperature and contraction. This effect is observed in the experiments, where the low-current arc shows a wider, less defined arc body (see figure 3). In addition, higher current can also increase the heating and therefore, "anchoring" the arc to a certain point or a "hot spot" [37].

3.2 Arc dynamics – modeling results

To explain the behavior of the gliding arc, the results from the 3D plasma model are presented and compared with the experiments. The main motivation is to gain insight into the arc movement and its shape and position.

The gas flow pattern, simulated with the SST model, is illustrated in figure 9. The results are represented as a streamline of the flow vector (figure 9(a)) and an arrow plot of a 2D cut-plane (figure 9(b)), for the configuration with anode diameter of 7.08 mm and a gas flow rate of 22 L/min.

It is clear that the gas, when entering the reactor, first moves upward in the cathode part (which has a larger diameter than the anode part) in an outer vortex, and when it arrives at the closed end of the cathode part (= top in figure 9(b)) it starts to flow downwards in a so-called reverse inner vortex with smaller diameter, because the gas has lost some rotational speed due to friction and inertia. This allows the gas to leave the reactor through the outlet (= anode part with smaller diameter).

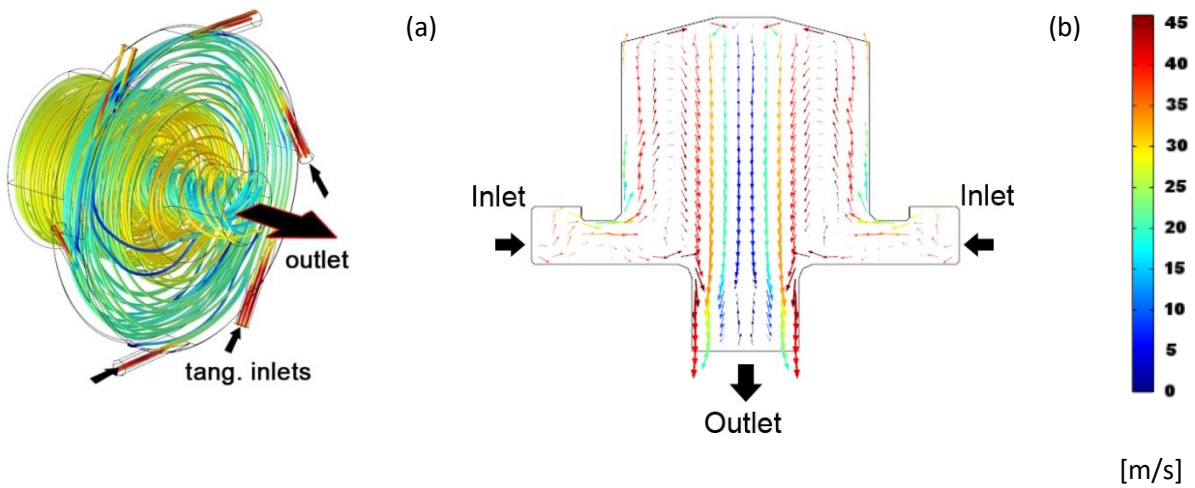

Figure 9. Streamline plot of the gas velocity and direction (a) and 2D arrow plot (b) illustrating the gas flow pattern.

The plasma simulation is performed using the gas flow data shown in figure 9 as a stationary solution and an arc current of 0.24 A. The convection coefficients from the particle and heat balance equations (see Supplementary Information) are directly derived from the flow vector, i.e. the arc moves in accordance with the gas flow. This can be clearly seen by visualizing the plasma density as a function of time.

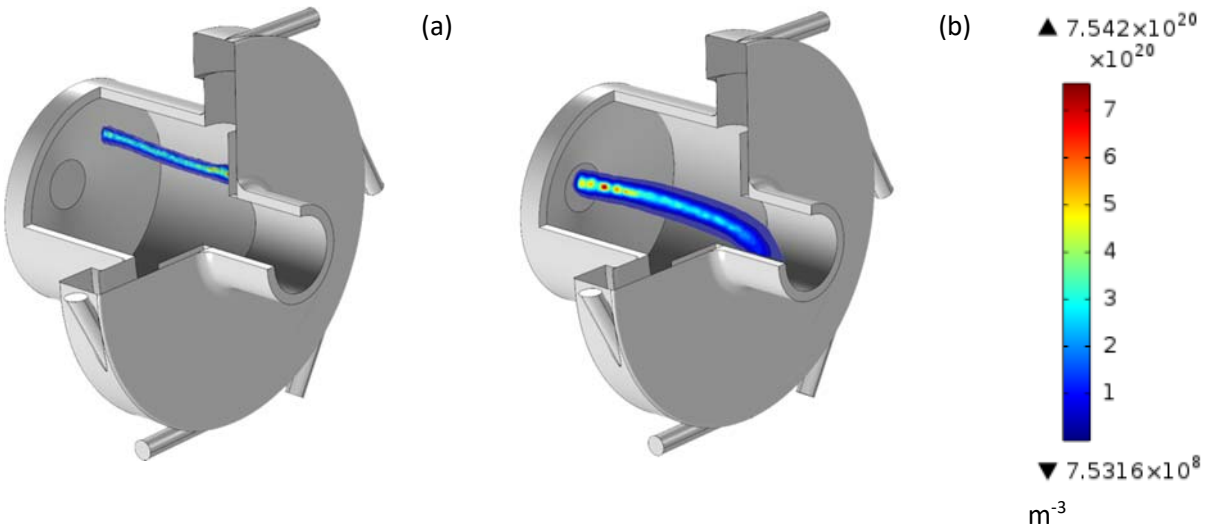

Figure 10. Calculated plasma density at an early stage of the arc at 2 ms (a) and a later stage at 4.6 ms (b).

As can be seen in figure 10, the arc is ignited at the shortest distance between the anode and the cathode (figure 10(a)), and it rotates in the reactor until it is stabilized in the reactor center by the flow (figure 10(b)). The plasma density has a value around 10^{20} m^{-3}, which is typical for non-thermal arc plasmas in argon. The main features of the arc shape are resolved – it is a bent column, with

characteristic hook-like attachment at the outlet (compare to figure 7). Nevertheless, we have to keep in mind that the arc shape in the model is only approximate, as it is limited by the resolution of the computational mesh.

The arc rotation can also be traced over time, after stabilization. In figure 11, this process is illustrated in frontal view for a full (360°) revolution. The calculated rotation period in the model is 0.7 ms for a gas flow rate of 22 L/min, which is in reasonable agreement with the experimental rotation period of 0.77 ms (i.e., rotation speed of 1300 rps; see figure 8).

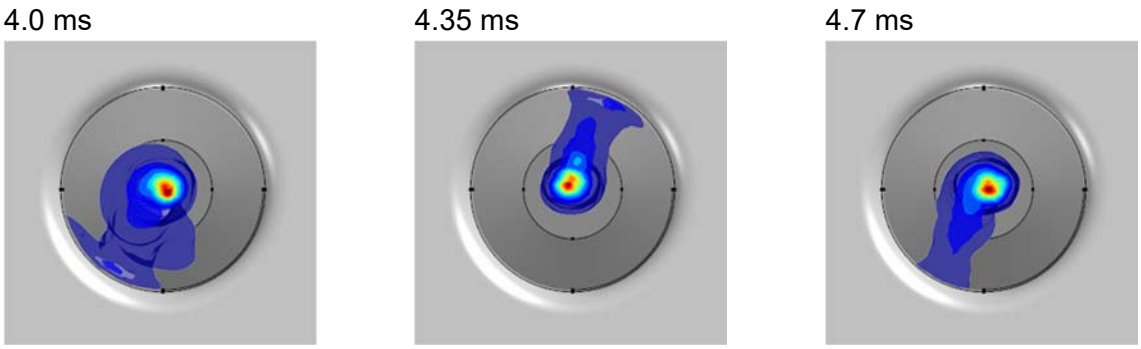

Figure 11. Arc position in frontal view, after stabilization in the reactor center, for a full rotation.

It is clear that several of the geometrical features of the arc, as observed in the high-speed photographs (see experimental section) are still missing from this simulation. In the model, the arc demonstrates a much simpler shape, resembling a bent column, while in the experiments many crooks and twists are present along its body, resembling a spiral spring. Computational limitations are the reason for this. First, the RANS flow model averages many of the turbulent vortices normally resulting in the flow, yielding a much smoother flow vector. This issue has been discussed before [37], and it can only be solved by significantly higher computational power, which is not available at the moment for the method in use, i.e. Comsol. Second, the discrete mesh density is limited, in order to provide reasonable computation times, which also leaves out many of the arc body details. Third, the boundary condition for the electrodes is adiabatic, meaning that they do not transfer heat. This effect can have an important influence, as already discussed in the experimental results section.

3.3 Influence of arc behavior on CO_2 conversion

To further improve the application of CO_2 conversion in a GAP, it is important to understand how the arc behavior influences this conversion. Therefore, we analyzed the feed and product gases by using gas chromatography. The conversion of CO_2, X_{CO_2}, is defined as:

$$X_{CO_2} = \frac{\dot{n}_{CO_2(in)} - \dot{n}_{CO_2(out)}}{\dot{n}_{CO_2(in)}} \times 100\% \quad (1)$$

where $\dot{n}_{CO_2(in)}$ and $\dot{n}_{CO_2(out)}$ are the molar flow rate of CO_2 without and with plasma, respectively. As the method mentioned above does not account for the gas expansion due to CO_2 splitting, a correction factor is used, which is explained in the Supporting Information of Ref. [33].

By measuring the plasma voltage and current, the plasma power can be calculated as follows:

$$P_{plasma} = \frac{1}{T}\int_0^{t=T} V_{plasma} \times I_{plasma} dt \quad (2)$$

In our case, the voltage and current are in phase.

In order to calculate the energy efficiency of CO_2 conversion, the specific energy input (SEI) in the plasma is defined as:

$$SEI\left(\frac{kJ}{L}\right) = \frac{Plasma\ power\ (kW)}{Flow\ rate\ (\frac{L}{min})} \times 60\left(\frac{s}{min}\right) \quad (3)$$

where the flow rate is expressed in L/min with reference conditions at a temperature of 0 °C and a pressure of 1 atm.

The energy efficiency of CO_2 conversion, η, is calculated as follows:

$$\eta(\%) = \frac{\Delta H_R\left(\frac{kJ}{mol}\right) \times X_{CO_2}(\%)}{SEI\left(\frac{kJ}{L}\right) \times 22.4\left(\frac{L}{mol}\right)} \quad (4)$$

where ΔH_R is the reaction enthalpy of CO_2 splitting (i.e., 279.8 kJ/mol), X_{CO_2} is the amount of CO_2 converted, SEI is defined above and 22.4 L/mol is the molar volume at 0 °C and 1 atm.

To elucidate how the arc behavior can influence the CO_2 conversion, we plot in figure 12 the CO_2 conversion (a), plasma power (b), SEI (c) and energy efficiency (d) for the different configurations at various operating conditions.

We showed before that the arc diameter increases with increasing anode diameter (see figure 4). This can lead to a drop in electron density as the same power is distributed over a larger volume, which can result in a lower conversion. Furthermore, when the anode diameter increases, the gas velocity and therefore also the rotation speed will decrease (see figure 8). Thus, there will be less mixing of plasma with the gas to be treated, so that less CO_2 can be converted. Another fact that indicates poor mixing in the configuration with larger anode diameter is the arc leaving the reactor. For the configuration with anode diameter of 7.08 mm the arc does not go outside of the reactor. However, as illustrated in figure 6, in the case of 14.20 mm and 17.50 mm the arc leaves the reactor lengthwise, as well as along the external face of the anode disk. The length of the arc that comes out of the reactor is similar for both cases, but the elongation along the external face of the anode disk clearly differs. In the configuration with anode diameter of 17.50 mm the arc moves all the way to the outer diameter of the anode, while in the case of 14.20 mm this elongation is limited. The arc leaving the reactor both lengthwise as well as towards the outer diameter of the anode has a negative effect on the conversion as there is less interaction of the plasma with the gas. All these effects, together with the fact that a smaller anode diameter leads to a more pronounced reverse vortex flow effect [33], explain why the reactor with smaller anode diameter gives rise to a higher CO_2 conversion and energy efficiency, as is indeed obvious from figure 12. The obtained CO_2 conversion is around 5.1 – 8.6 % (rising with decreasing flow rate), while the energy efficiency is 30 – 35 % (rising with increasing flow rate).

Figure 12 indeed illustrates, also for the other configurations, that a lower gas flow rate gives rise to a higher conversion, but a lower energy efficiency. This is merely attributed to the longer residence time of the gas in the plasma (for the conversion) and to the higher specific energy input (for the energy efficiency), and not so much to the arc dynamics itself. Indeed, the arc diameter does not change as a function of the gas flow rate. Furthermore, the effect of gas flow rate on the rotation speed and length of the arc coming out of the reactor for the configurations with anode diameter of 14.20 mm and 17.50 mm is also negligible. For the configuration with anode diameter of 7.08 mm, the rotation speed increases with increasing gas flow rate. In this respect, we would expect that the conversion would increase because of a better mixing. However, the results indicate that the effect

of the residence time has a larger contribution than the latter effect, which leads to a lower conversion for a higher flow rate. Since the plasma power is rather constant for each gas flow rate (see figure 12(b)), it is logical that the SEI decreases with increasing gas flow rate (figure 12(c)). As a consequence, the energy efficiency rises with increasing gas flow rate (figure 12(d)).

Finally, if we compare the effect of electric current, for the configuration with anode diameter of 14.20 mm, it is clear from figure 12 that a higher electric current results in more CO_2 conversion. The arc diameter is more or less the same for both cases (see figure 4), while the rotation speed increases only slightly upon rising electric current (see figure 8). However, these two currents form a different regime, as discussed in [33]. Figure 3 clearly shows that the arc is less bright for an electric current of 0.05 A compared to 0.35 A. Hence, there is less excitation, due to the lower electron density, and therefore also a lower conversion, as indeed illustrated in figure 12(a). This last phenomenon is also observed for the plasma power (figure 12 (b)). The plasma power is lower at an input current of 0.05 A compared to 0.35 A. This can be correlated with the observation that the arc is less bright for an input current of 0.05 A, and it supports our assumption that there is less excitation in this plasma regime. For some flow rates, the energy efficiency is higher at an input current of 0.05 A compared to 0.35 A. However, the corresponding conversion in these cases is quite low (figure 12 (a)). Therefore, these cases are overall not so interesting for CO_2 conversion [33].

The CO_2 conversion and energy efficiency obtained in these experiments are quite promising, also when compared to other plasma reactors, including other types of gliding arcs. A detailed comparison of these results with data from literature for other plasma reactors was presented in our previous paper [33].

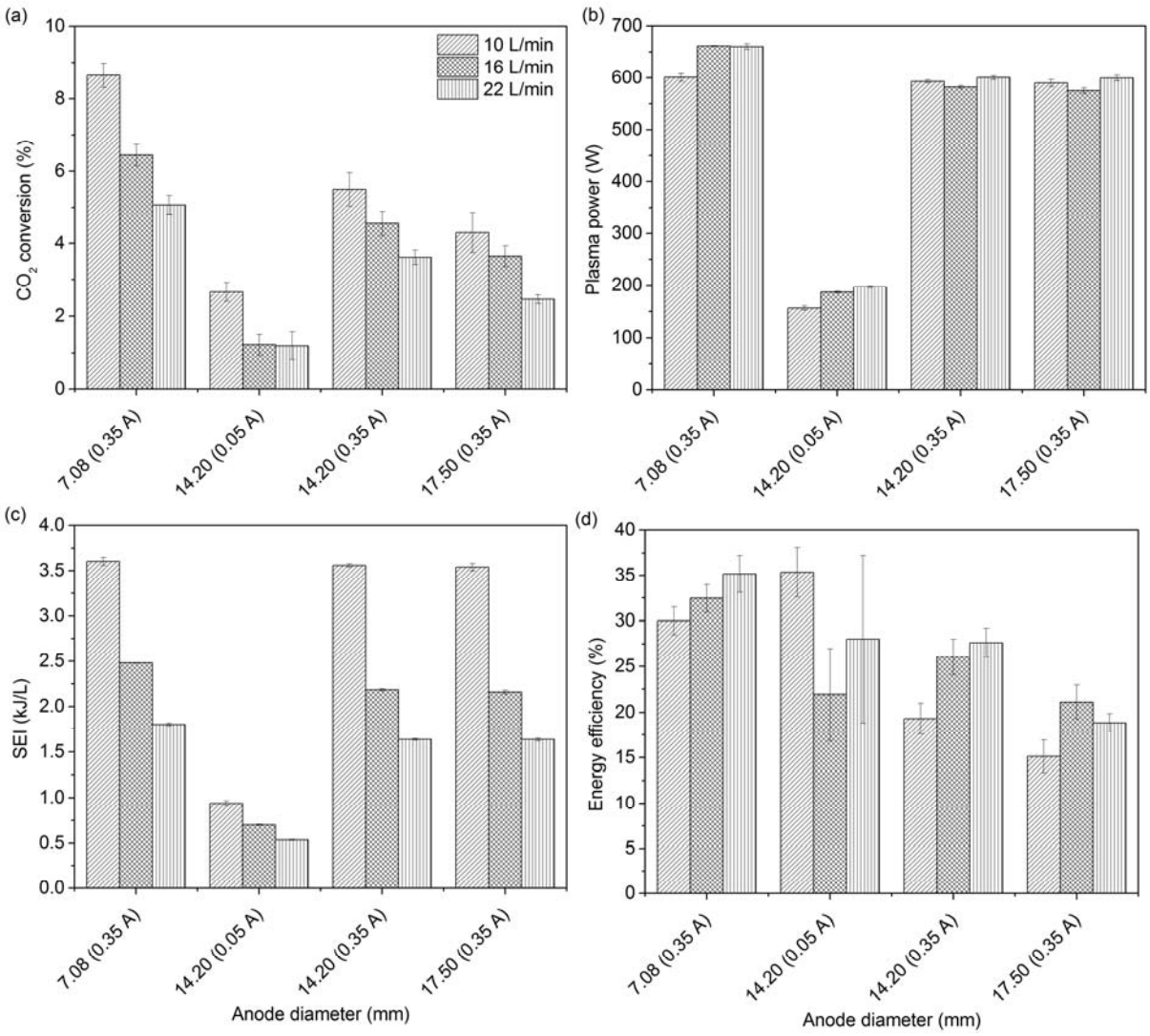

Figure 12. CO_2 conversion (a), plasma power (b), SEI (c) and energy efficiency (d) for the different configurations at various operating conditions.

4. Conclusion

We present here the arc dynamics of a novel type of gliding arc discharge, i.e., the Gliding Arc Plasmatron (GAP), which has reverse vortex flow stabilization, and we also discuss the effects of the gliding arc dynamics on the CO_2 conversion capabilities. We present for the first time high-speed camera images, which illustrate the arc stabilization process and the arc geometrical features in a GAP. Clearly, the arc movement and shape relies on a number of factors, such as gas turbulence, outlet diameter, electrode surface, gas contraction and buoyance force. We present results for different gas flow rates, arc currents and anode (outlet) diameters, showing how these parameters affect the arc diameter, rotation speed and elongation. In addition, we compare the experimental images to a state-of-art 3D-plasma model, which predicts the plasma movement and rotation speed with very good accuracy. Finally, we correlate the arc dynamics with the CO_2 conversion and energy efficiency, at exactly the same conditions, to explain the effect of these parameters on the CO_2 conversion process. This work is important for understanding and optimizing the GAP for CO_2 conversion.

Acknowledgements

This work was supported by the Belgian Federal Office for Science Policy (BELSPO) and the Fund for Scientific Research Flanders (FWO; grant numbers G.0383.16N and 11U5316N).

References

[1] A. Bogaerts, E. Neyts, R. Gijbels, J. van der Mullen, Gas discharge plasmas and their applications, Spectrochim. Acta, Part B. 57 (2002) 609–658.

[2] J. Van Durme, J. Dewulf, W. Sysmans, C. Leys, H. Van Langenhove, Efficient toluene abatement in indoor air by a plasma catalytic hybrid system, Appl. Catal. B Environ. 74 (2007) 161–169.

[3] K. Van Wesenbeeck, B. Hauchecorne, S. Lenaerts, Study of positive and negative plasma catalytic oxidation of ethylene, Environ. Technol. (2016) DOI:10.1080/09593330.2016.1237553.

[4] R. Snoeckx, A. Bogaerts, Plasma technology - a novel solution for CO2 conversion?, Chem. Soc. Rev. 46 (2017) 5805-5863

[5] R. Aerts, W. Somers, A. Bogaerts, Carbon Dioxide Splitting in a Dielectric Barrier Discharge Plasma: A Combined Experimental and Computational Study, ChemSusChem. 8 (2015) 702–716.

[6] R. Aerts, R. Snoeckx, A. Bogaerts, In-Situ Chemical Trapping of Oxygen in the Splitting of Carbon Dioxide by Plasma, Plasma Process. Polym. 11 (2014) 985–992.

[7] R. Aerts, T. Martens, A. Bogaerts, Influence of Vibrational States on CO2 Splitting by Dielectric Barrier Discharges, J. Phys. Chem. C. 116 (2012) 23257–23273.

[8] M. Ramakers, I. Michielsen, R. Aerts, V. Meynen, A. Bogaerts, Effect of argon or helium on the CO2 conversion in a dielectric barrier discharge, Plasma Process. Polym. 12 (2015) 755–763.

[9] F. Brehmer, S. Welzel, M.C.M. Van De Sanden, R. Engeln, CO and byproduct formation during CO2 reduction in dielectric barrier discharges, J. Appl. Phys. 116 (2014) 123303.

[10] K. Van Laer, A. Bogaerts, Improving the Conversion and Energy Efficiency of Carbon Dioxide Splitting in a Zirconia-Packed Dielectric Barrier Discharge Reactor, Energy Technol. 3 (2015) 1038–1044.

[11] T. Kozák, A. Bogaerts, Splitting of CO_2 by vibrational excitation in non-equilibrium plasmas: a reaction kinetics model, Plasma Sources Sci. Technol. 23 (2014) 45004.

[12] T. Silva, N. Britun, T. Godfroid, R. Snyders, Optical characterization of a microwave pulsed discharge used for dissociation of CO 2, Plasma Sources Sci. Technol. 23 (2014) 25009.

[13] S. Heijkers, R. Snoeckx, T. Kozák, T. Silva, T. Godfroid, N. Britun, R. Snyders, A. Bogaerts, CO 2 conversion in a microwave plasma reactor in the presence of N 2 : modelling and experimental validation O-15-6 O-15-6, J. Phys. Chem. C. 119 (2015) 12815–12828.

[14] A. Indarto, J.-W. Choi, H. Lee, H.K. Song, Conversion of CO2 by gliding arc plasma, Environ.

Eng. Sci. 23 (2006) 1033–1043.

[15] A. Indarto, D.R. Yang, J.W. Choi, H. Lee, H.K. Song, Gliding arc plasma processing of CO2 conversion, J. Hazard. Mater. 146 (2007) 309–315.

[16] T. Nunnally, K. Gutsol, A. Rabinovich, A. Fridman, A. Gutsol, A. Kemoun, Dissociation of CO2 in a Low Current Gliding Arc Plasmatron, J. Phys. D. Appl. Phys. 44 (2011) 274009.

[17] L.F. Spencer, A.D. Gallimore, Efficiency of CO 2 dissociation in a radio-frequency discharge, Plasma Chem. Plasma Process. 31 (2011) 79–89.

[18] L.F. Spencer, A.D. Gallimore, CO 2 dissociation in an atmospheric pressure plasma/catalyst system: a study of efficiency, Plasma Sources Sci. Technol. 22 (2013) 15019.

[19] R.I. Asisov, A.K. Vakar, V.K. Jivotov, M.F. Krotov, O.A. Zinoviev, B.V. Potapkin, A.A. Rusanov, V.D. Rusanov, A.A. Fridman, Non-equilibrium plasma-chemical process of CO2 decomposition in a supersonic microwave discharge, Proc. USSR Acad. Sci. 271 (1983).

[20] V.D. Rusanov, A. Fridman, G.V. Sholin, The physics of a chemically active plasma with nonequilibrium vibrational excitation of molecules, Sov. Phys. Usp. 24 (1981) 447–474.

[21] G.J. van Rooij, D.C.M. van den Bekerom, N. den Harder, T. Minea, G. Berden, W.A. Bongers, R. Engeln, M.F. Graswinckel, E. Zoethout, M.C.M. van de Sanden, Taming microwave plasma to beat thermodynamics in CO2 dissociation., Faraday Discuss. 183 (2015) 233–248.

[22] W. Bongers et al., Plasma-driven dissociation of CO 2 for fuel synthesis, Plasma Process. Polym. (2016) DOI: 10.1002/ppap.201600126.

[23] J.L. Liu, H.W. Park, W.J. Chung, D.W. Park, High-Efficient Conversion of CO2 in AC-Pulsed Tornado Gliding Arc Plasma, Plasma Chem. Plasma Process. 36 (2015) 437–449.

[24] M.S. Bak, S.K. Im, M. Cappelli, Nanosecond-pulsed discharge plasma splitting of carbon dioxide, IEEE Trans. Plasma Sci. 43 (2015) 1002–1007.

[25] Q. Yu, M. Kong, T. Liu, J. Fei, X. Zheng, Characteristics of the decomposition of CO 2 in a dielectric packed-bed plasma reactor, Plasma Chem. Plasma Process. 32 (2012) 153–163.

[26] S. Paulussen, B. Verheyde, X. Tu, C. De Bie, T. Martens, D. Petrovic, A. Bogaerts, B. Sels, Conversion of carbon dioxide to value-added chemicals in atmospheric pressure dielectric barrier discharges, Plasma Sources Sci. Technol. 19 (2010) 034015 1-6.

[27] X. Tu, J.C. Whitehead, Plasma dry reforming of methane in an atmospheric pressure AC gliding arc discharge: Co-generation of syngas and carbon nanomaterials, Int. J. Hydrogen Energy. 39 (2014) 9658–9669.

[28] A. Fridman, Plasma Chemistry, Cambridge University Press, New York, 2008.

[29] A. Indarto, J. Choi, H. Lee, H.K. Song, Conversion of CO 2 by Gliding Arc Plasma, Environ. Eng. Sci. 23 (2006) 1033–1043.

[30] A. Indarto, J.W. Choi, H. Lee, H.K. Song, Effect of additive gases on methane conversion using

gliding arc discharge, Energy. 31 (2006) 2986–2995.

[31] X. Tao, M. Bai, X. Li, H. Long, S. Shang, Y. Yin, X. Dai, CH4–CO2 reforming by plasma – challenges and opportunities, Prog. Energy Combust. Sci. 37 (2011) 113–124.

[32] G. Petitpas, J.D. Rollier, A. Darmon, J. Gonzalez-Aguilar, R. Metkemeijer, L. Fulcheri, A comparative study of non-thermal plasma assisted reforming technologies, Int. J. Hydrogen Energy. 32 (2007) 2848–2867.

[33] M. Ramakers, G. Trenchev, S. Heijkers, W. Wang, A. Bogaerts, Gliding Arc Plasmatron: providing an alternative method for carbon dioxide conversion, Chem. Sus. Chem. 10 (2017) 2642–2652.

[34] A. Gutsol, A. Rabinovich, A. Fridman, Combustion-assisted plasma in fuel conversion, J. Phys. D. Appl. Phys. 44 (2011) 274001.

[35] S.R. Sun, H.X. Wang, D.H. Mei, X. Tu, A. Bogaerts, CO2 conversion in a gliding arc plasma: performance improvement based on chemical reaction modeling, J. CO2 Util. 17 (2017) 220–234.

[36] S. Kolev, A. Bogaerts, A 2D model for a gliding arc discharge, Plasma Sources Sci. Technol. 24 (2015) 15025.

[37] G. Trenchev, S. Kolev, A. Bogaerts, A 3D model of a reverse vortex flow gliding arc reactor, Plasma Sources Sci. Technol. 25 (2016) 35014.

[38] X. Tu, H.J. Gallon, J.C. Whitehead, Dynamic behavior of an atmospheric argon gliding arc plasma, IEEE Trans. Plasma Sci. 39 (2011) 2900–2901.

[39] J. Zhu, J. Gao, A. Ehn, M. Aldén, Z. Li, D. Moseev, Y. Kusano, M. Salewski, A. Alpers, P. Gritzmann, M. Schwenk, Measurements of 3D slip velocities and plasma column lengths of a gliding arc discharge, Appl. Phys. Lett. 106 (2015) 44101.

[40] G. Trenchev, S. Kolev, W. Wang, M. Ramakers, A. Bogaerts, CO2 Conversion in a Gliding Arc Plasmatron: Multi-Dimensional Modelling for Improved Efficiency, J. Phys. Chem. C. Submitted.

[41] COMSOL 5.0, (n.d.). https://www.comsol.com.

[42] F.R. Menter, M. Kuntz, R. Langtry, Ten Years of Industrial Experience with the SST Turbulence Model, Turbul. Heat Mass Transf. 4. 4 (2003) 625–632.

[43] D.C. Wilcox, Turbulence Modeling for CFD, Third Edit, DCW Industries, 2006.